

# One-Step Synthesis of Magnetic Zeolite from Zinc Slag and Circulating Fluidized Bed Fly Ash for Degradation of Dye Wastewater

Zhichao Han, Yaojun Zhang\* and Panyang He

College of Materials Science and Engineering, Xi'an University of Architecture and Technology, Xi'an, 710055, China

\*Corresponding Author: Yaojun Zhang. Email: zhangyaojun@xauat.edu.cn

Received: 05 December 2019; Accepted: 13 February 2020

**Abstract:** In this study, a magnetic P zeolite was directly synthesized by utilization of industrial solid wastes of zinc slag (ZS) and circulating fluidized bed fly ash (CFBFA) via one-step hydrothermal method. The effects of different CFBFA/ZS ratios and hydrothermal times on the as-synthesized zeolite were investigated. The X-ray diffraction (XRD) and vibrating sample magnetometer (VSM) results indicated that the magnetic P zeolite possessed well-defined crystals and superparamagnetism. The as-prepared zeolite was employed as a Fenton-like solid catalyst for degradation of direct green B dye wastewater. It was discovered that the magnetic P zeolite took the advantage of rapid separation and efficient recovery under the external magnets in a solid-liquid reaction. The effects of the solution pH, the catalyst dosage, and the H<sub>2</sub>O<sub>2</sub> concentration on the degradation rate of direct green B dye wastewater were studied systematically. The results showed that the highest degradation of 96.3% was obtained and the magnetic P zeolite showed excellent stability after four cycles. Therefore, the magnetic P zeolite derived from industrial solid wastes had a potential application in wastewater treatment.

**Keywords:** Magnetic zeolite; solid wastes; Fenton-like reaction; dye degradation

## 1 Introduction

Zeolite, a type of aluminosilicate material with regular channels and unique crystal structure, has been widely used in the fields of petrochemical industry, fine chemical industry and environmental protection due to its excellent ion exchange, catalysis and adsorption properties [1,2]. However, the synthesized zeolites are usually solid powders which are difficult to be separated in the solid-liquid system so that the wide applications of zeolite powders have been limited. Magnetic zeolite powders have the advantages of easy separation and recycling by use of the magnetic technology, and become a research hotspot in the water treatment. Yamaura et al. [3,4] reported that the hydroxyl sodalite was synthesized by the hydrothermal reaction of fly ash and NaOH solution at 100°C for 24 h, and then the magnetic composite was obtained by blending of hydroxyl sodalite with magnetic Fe<sub>3</sub>O<sub>4</sub> by a mass ratio of 3:1 in aqueous solution. Anunziata et al. [5] synthesized a magnetic Fe<sup>n+</sup>-ZSM-11 zeolite by the incipient wetness impregnation of FeSO<sub>4</sub>•7H<sub>2</sub>O and Fe(NO<sub>3</sub>)<sub>3</sub>•9H<sub>2</sub>O salt solutions on the surface of NH<sub>4</sub>-ZSM-11 zeolite, and then heated at 500°C for 10 h under nitrogen atmosphere and



This work is licensed under a Creative Commons Attribution 4.0 International License, which permits unrestricted use, distribution, and reproduction in any medium, provided the original work is properly cited.

calcined in air at 500°C for 12 h. Cao et al. [6] reported that some pure chemical reagents were mixed at a molar ratio of  $\text{Na}_2\text{O}:\text{Al}_2\text{O}_3:\text{SiO}_2:\text{H}_2\text{O} = 3:1:2.3:185$ , and then blended with magnetic  $\text{Fe}_3\text{O}_4$  to get a mixture which was heated at 95°C for 6 h to obtain a magnetic P-type zeolite.

As mentioned above, the magnetic zeolites are usually achieved by addition of magnetic oxide into the as-synthesized zeolites, in which two or more steps are required in the preparation of magnetic zeolites. Recently, Belviso et al. [7] reported that a mixture of waste materials (fly ash and red mud) and NaOH at a mass ratio of 1:1.2 was fused at 600°C for 12 h, and then the molten material was mixed with distilled water which was incubated at 25–40°C for 4 days to acquire a mixture of A-, X- and ZK-5-type magnetic zeolites without the addition of iron oxide magnetic nanoparticles.

Zinc slag (ZS) is an industrial solid waste discharged from the zinc smelting process. The China Report Hall [8] reported that the output of zinc metal was 5.681 million tons in 2018. The discharge of zinc slag in China was about 5.45 million tons, and its historical stockpiling volume exceeded to 100 million tons according to the production of each ton of zinc metal to discharge 0.96 tons of zinc slag [9]. Circulating fluidized bed boiler (800–900°C) is a new clean combustion technology of high efficiency and low pollution. It is reported that the annual discharge of circulating fluidized bed fly ash (CFBFA) is about 90 million tons and gradually increases year by year [10]. The vast accumulation of ZS and CFBFA has already caused wasting of resources, serious environmental pollution, and huge economic losses [11,12]. This paper takes a mixture of ZS and CFBFA as silicon and aluminum sources, and utilizes the magnetic component containing in the ZS and CFBFA to directly synthesize magnetic P zeolite without addition of magnetic oxide via one-step hydrothermal reaction. The utilization of industrial solid wastes as precursors for preparation of zeolites can not only reduce the environmental pressure, but also obtain high value-added magnetic zeolite. Moreover, the magnetic P zeolite synthesized from ZS and CFBFA is employed as a Fenton-like catalyst for the simulated degradation of printing and dyeing wastewater. It can be a new approach to achieve the dual purpose of “waste control by waste”. To our knowledge, the study on utilization of ZS and CFBFA as precursors for the direct synthesis of magnetic P zeolite by one-step hydrothermal reaction has not yet been reported in the current literatures.

## 2 Materials and Methods

### 2.1 Materials

The zinc slag (ZS) was provided by Zinc Smelting Plant of Shangluo, Shaanxi province of China and the circulating fluidized bed fly ash (CFBFA) was from Shenhua Junggar Energy Corporation in Junggar, Inner Mongolia of China. The main chemical components of ZS and CFBFA were measured by the weight percent using X-ray fluorescence (XRF) and listed in Tab. 1. The sodium hydroxide (A. R.) was purchased from Xi'an Chemical Reagent Company. The water is deionized water.

**Table 1:** Chemical composition of CFBFA and ZS

Sample	CaO	SiO <sub>2</sub>	Al <sub>2</sub> O <sub>3</sub>	Fe <sub>2</sub> O <sub>3</sub>	MgO	Na <sub>2</sub> O	K <sub>2</sub> O	SO <sub>3</sub>	TiO <sub>2</sub>
CFBFA	2.87	35.14	45.35	2.61	0.23	0.08	0.34	0.54	1.82
ZS	9.10	16.79	8.94	39.68	2.32	1.00	4.00	0.42	–

### 2.2 Synthesis of Magnetic Zeolite

The ZS, CFBFA, NaOH and water at the mass ratio of 0.66:1:0.73:15 were weighed respectively. The ZS and CFBFA were thoroughly blended to form a mixture which was poured into 1.2 mol/L NaOH solution and stirred for 2 min to become homogeneous slurry, and then the slurry was placed into a 200 mL of

autoclave to carry out the hydrothermal reaction at 105°C for 12 h, 24 h, 48 h and 60 h, respectively. The different magnetic P zeolite samples were obtained after filtration, washing and drying. The different ratios of CFBFA and ZS were shown in [Tab. 2](#).

**Table 2:** Composition of CFBFA and ZS mixture

Sample	CFBFA (wt%)	ZS (wt%)	Si/Al
CZ(20/80)*	20	80	1.07
CZ(60/40)*	60	40	0.76
CZ(80/20)*	80	20	0.70

\* The samples of CZ(80/20), CZ(60/40) and CZ(20/80) were synthesized at the different ratios of CFBFA and ZS by the weight percent (The acronym of CZ is from the first letters both CFBFA and ZS).

### 2.3 Characterization of Magnetic Zeolites

Elemental analysis of the sample was carried out on an X-ray fluorescence spectrometer. The X-ray diffraction (XRD) patterns of the samples were recorded on an X-ray diffractometer using  $\text{CuK}\alpha$  ( $\lambda = 1.54056 \text{ \AA}$ ) operated at 40 kV and 40 mA with a scanning rate of  $10^\circ/\text{min}$  from  $2\theta$  range of  $5\text{--}70^\circ$ . The micro-morphologies were captured by a FEI Quanta 200 scanning electron microscopy (SEM) equipped with energy dispersive X-ray spectroscopy (EDS). Fourier-transform infrared (FT-IR) spectra of samples were detected on a Nicolet 5700 FT-IR spectrophotometer in the range of  $400$  to  $4000 \text{ cm}^{-1}$  using a KBr disk. The magnetization hysteresis loop of sample was determined on a VSM-7404 type vibrating sample magnetometer.

### 2.4 Treatment of Printing and Dyeing Wastewater

The catalytic activities of magnetic P zeolites were evaluated by simulated degradation of printing and dyeing wastewater of direct green B dye in Fenton-like reaction. The initial absorbance ( $A_0$ ) of direct green B dye (the corresponding concentration ( $C_0$ )) was measured at the maximum absorption wavelength of 628 nm. Put 100 mL of direct green B dye solution with concentration of 40 mg/L into a beaker, and then add certain amount of  $\text{H}_2\text{O}_2$  into the solution. The pH value of solution was adjusted by addition of 0.1 M HCl or 0.05 M NaOH. After a certain amount of magnetic P zeolite was introduced to the solution containing direct green B dye, the solution was stirred at 200 rpm for certain time. The supernatant solution was obtained by centrifugal separation at 10 min intervals and was monitored the absorbance ( $A_t$ ) (the corresponding concentration ( $C_t$ )). The degradation rate (DR) of dye was calculated using [Eq. \(1\)](#). Where  $DR$  is the degradation rate of direct green B dye,  $A_0$  ( $C_0$ ) and  $A_t$  ( $C_t$ ) are the absorbance (concentration) of direct green B dye solution at original and  $t$  time, respectively.

$$DR (\%) = (C_0 - C_t) / C_0 \times 100\% = (A_0 - A_t) / A_0 \times 100\% \quad (1)$$

## 3 Results and Discussion

### 3.1 Microstructure of Magnetic P Zeolite

[Fig. 1](#) shows the XRD patterns of samples. From the [Fig. 1a](#), it can be found that the CFBFA sample displays several diffraction peaks at  $20.85^\circ$ ,  $26.74^\circ$  as well as at  $16.28^\circ$ ,  $26.47^\circ$ ,  $33.29^\circ$ ,  $40.90^\circ$ ,  $45.63^\circ$ ,  $67.39^\circ$  belonging to quartz and mullite phases, respectively, and the broad diffuse hump in the range of  $15^\circ\text{--}35^\circ$  is assigned to be amorphous silica. In the pattern of ZS, there are the characteristic peaks of magnetite at  $30.1^\circ$ ,  $43.1^\circ$  and  $53.5^\circ$  (JCPDS No. 74-0748), besides the quartz and mullite phases. [Fig. 1b](#) presents the XRD patterns of samples synthesized from the different ratios of CFBFA to ZS by the weight percent which are shown in [Tab. 2](#). For the CZ(20/80) sample, some peaks occur at  $12.42^\circ$ ,

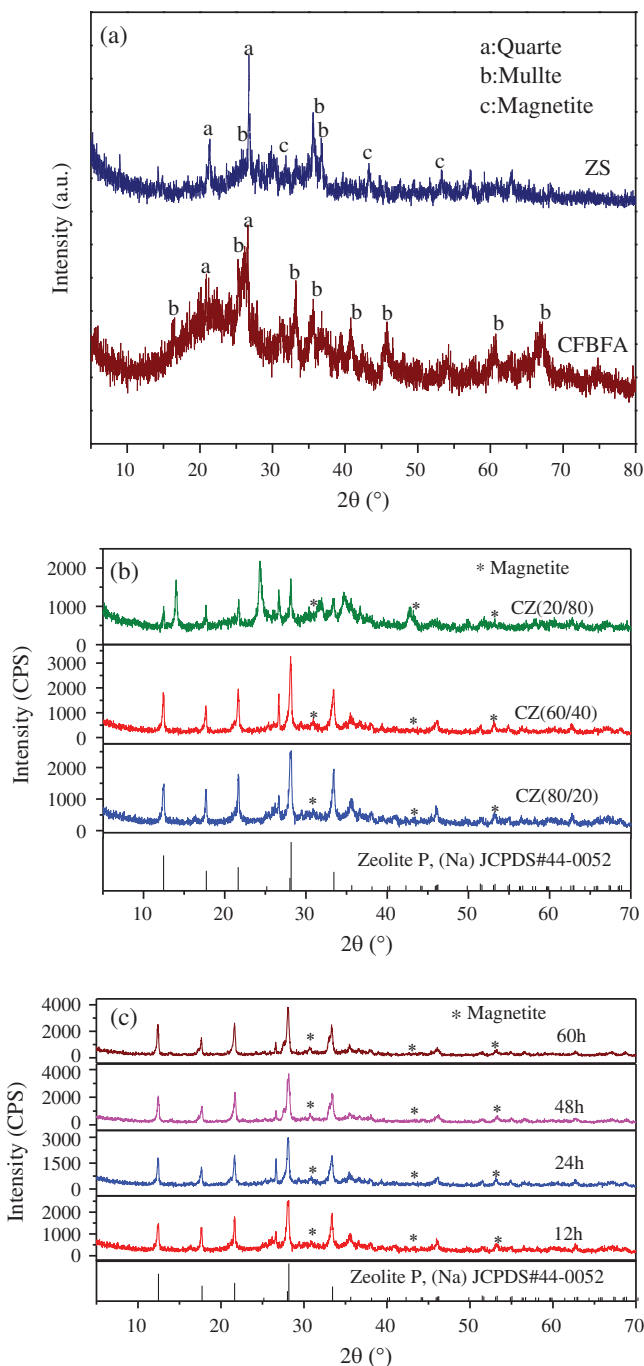


**Figure 1:** XRD patterns of samples. (a) Raw materials of CFBFA and ZS, (b) Samples of CZ(80/20), CZ(60/40) and CZ(20/80) synthesized from the different ratios of CFBFA to ZS by the weight percent, and (c) Crystallization times of CZ(60/40) from 12 h, 24 h, 48 h to 60 h, respectively

17.63°, 21.61°, 28.04°, 33.35° and 46.02° corresponding to P zeolite (JCPDS No.44–0052), and others appear at 30.1°, 43.1° and 53.5° to be the magnetite ( $\text{Fe}_3\text{O}_4$ ) (JCPDS No. 74–0748), indicating that the magnetic P zeolite is successfully synthesized by one-step hydrothermal reaction. When the weight percent of CFBFA is gradually increasing from 20 to 80 in the different samples, it is clear that the peak

intensities of P zeolite display a trend of increasing first, but then decreasing. The pattern of CZ(60/40) has a set of the highest intensity of peaks. Fig. 1c shows the patterns of the CZ(60/40) sample at different crystallization times from 12 h, 24 h, 48 h to 60 h. It can be seen that the peak intensities of P zeolite are rapidly increasing from 12 h to 48 h, and then approach to constant value at 60 h, demonstrating that the optimal mass ratio of ZS:CFBFA:NaOH:H<sub>2</sub>O = 0.66:1:0.73:15, and the hydrothermal time of 48 h are critical for the synthesis of magnetic P zeolite.

Fig. 2 displays SEM micrographs of the samples. The CFBFA shows the irregular particles with size about 30  $\mu\text{m}$  in Fig. 2a, and ZS also exhibits an irregular morphology with size about 20  $\mu\text{m}$  in Fig. 2b. From Fig. 2c–2f, a kind of spherical crystals are obtained and identified as P zeolite, which are similar to those reported in previous literatures [13,14]. In addition, it is revealed that the increasing of crystallization time from 12 h to 60 h is beneficial to the formation of magnetic P zeolite spherical particles with mean size about 2  $\mu\text{m}$ . In comparison with CFBFA and ZS, the magnetic P zeolites show relatively much smaller and more uniform spherical particles. The previous studies also reported that the particle size of P zeolite is about 2–10  $\mu\text{m}$  [13,14]. During the hydrothermal treatment, the silicon and aluminum species in CFBFA and ZS are dissolved in NaOH solution to form  $[\text{SiO}_4]^{4-}$  and  $[\text{AlO}_4]^{5-}$  tetrahedrons which are the primary building block of zeolite, and then the micro-crystals of P zeolite are obtained under the template agent of  $\text{Na}^+$  ions [15]. Furthermore, the EDS result indicates that the presence of Fe, Si, Al and O in the P zeolites. SEM and EDS results further demonstrate the creation of magnetic P zeolite.

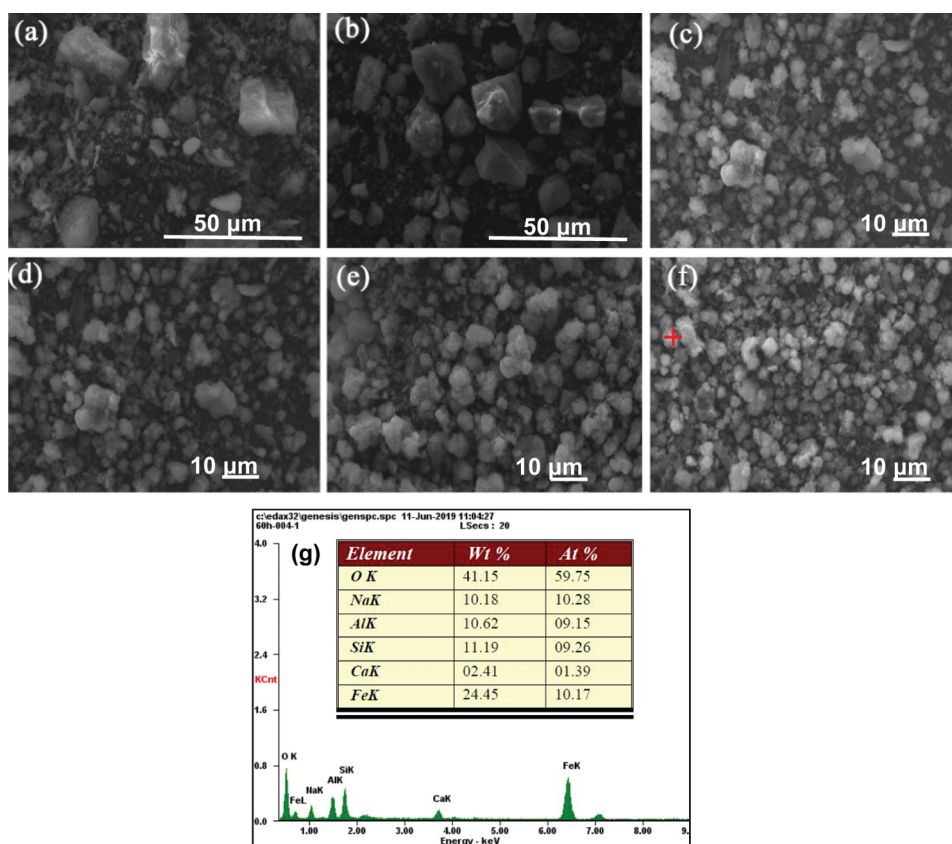


**Figure 2:** SEM micrographs of (a) CFBFA, (b) ZS, (c–f) crystallization times of magnetic P zeolite sample (CZ(60/40)) from 12 h, 24 h, 48 h to 60 h as well as the element analysis of EDS

Fig. 3 shows the FT-IR spectra of ZS, CFBFA and magnetic P zeolite that there are a wide peak at the high frequency region from 3429 to 3448  $\text{cm}^{-1}$  for each sample corresponding to the stretching vibration of O-H bond, and a weak peak at intermediate frequency region from 1624 to 1645  $\text{cm}^{-1}$  associating with the bending vibration of O-H bond, respectively [16]. In the spectrum of ZS, there are two peaks at 1041  $\text{cm}^{-1}$  and 467  $\text{cm}^{-1}$  which are attributed to antisymmetric stretching and bending vibrations of Si-O, and the band at 606  $\text{cm}^{-1}$  is assigned to the Fe-O stretching mode of the tetrahedral and octahedral sites in magnetite [17]. The CFBFA presents a series of bands deriving from antisymmetric stretching vibration of Si-O at 1097  $\text{cm}^{-1}$ , symmetric vibration of Si-O-Si and Al-O in mullite-like structures at 821  $\text{cm}^{-1}$ , stretching vibration of Al(VI)-O-Si at 566  $\text{cm}^{-1}$ , and Si-O bending vibration at 469  $\text{cm}^{-1}$  [18,19]. In the spectrum of the magnetic P zeolite, the peak at 606  $\text{cm}^{-1}$  ascribes to the Fe-O stretching mode, and the band at 739  $\text{cm}^{-1}$  is attributed to the symmetric stretching vibration of the internal tetrahedrons [20]. The peaks at about 981  $\text{cm}^{-1}$  and 430  $\text{cm}^{-1}$  belong to the internal vibrations of Si(Al)O<sub>4</sub> tetrahedrons in P zeolite [21,22]. The above results also demonstrate the formation of magnetic P zeolite.

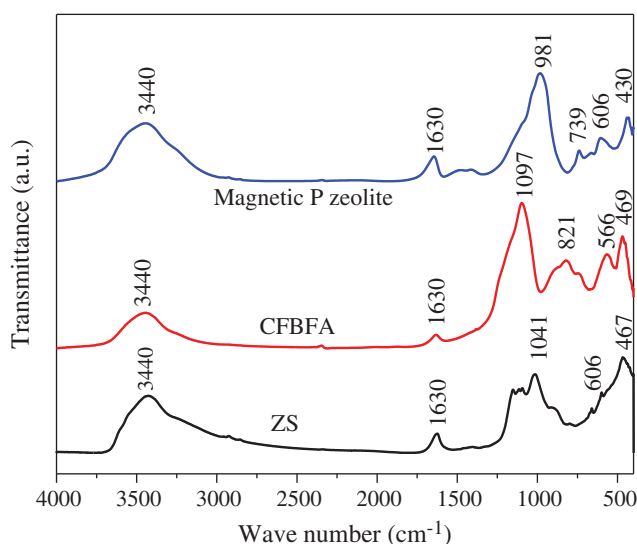
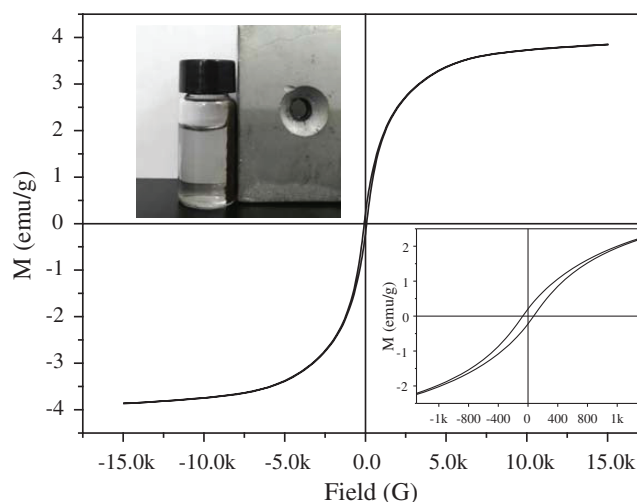


Figure 3: FT-IR spectra of samples

### 3.2 The Magnetic Properties of P Zeolite

Fig. 4 shows the hysteresis loop of the magnetic P zeolite measured by a vibrating sample magnetometer. The hysteresis loops of magnetic P zeolite presents the curve of S-like shape. The magnetization of the magnetic P zeolite increases with increasing of applied magnetic field and tends to saturation at high intensity, while the magnetization gradually decreases and approaches to zero as the applied magnetic field slowly reduces from high intensity to zero, so do the applied magnetic field in reverse. In addition, the magnetic P zeolite has a small coercive force of 70.02 G and a remanence of 0.05 emu/g, which indicates that the magnetic P zeolite has superparamagnetism. The special saturation magnetization (M) of 3.85 emu/g testifies that the magnetic P zeolite has a promising application in the magnetic separation technology of wastewater treatment. Belviso et al. [7] and Cao et al. [13] reported that the magnetic zeolite with a saturation magnetization (M) of 2 emu/g and 2.88 emu/g were synthesized, respectively. Jiang et al. [23] prepared magnetic zeolite of P/Ni/wollastonite composite fibers with a saturation magnetization (M) of 1.81 emu/g. It is clear that the saturation magnetization of the as-prepared P zeolite is slightly higher than that of magnetic zeolites reported in previous literatures, meaning that the magnetic P zeolite can be more quickly attracted towards a magnet.



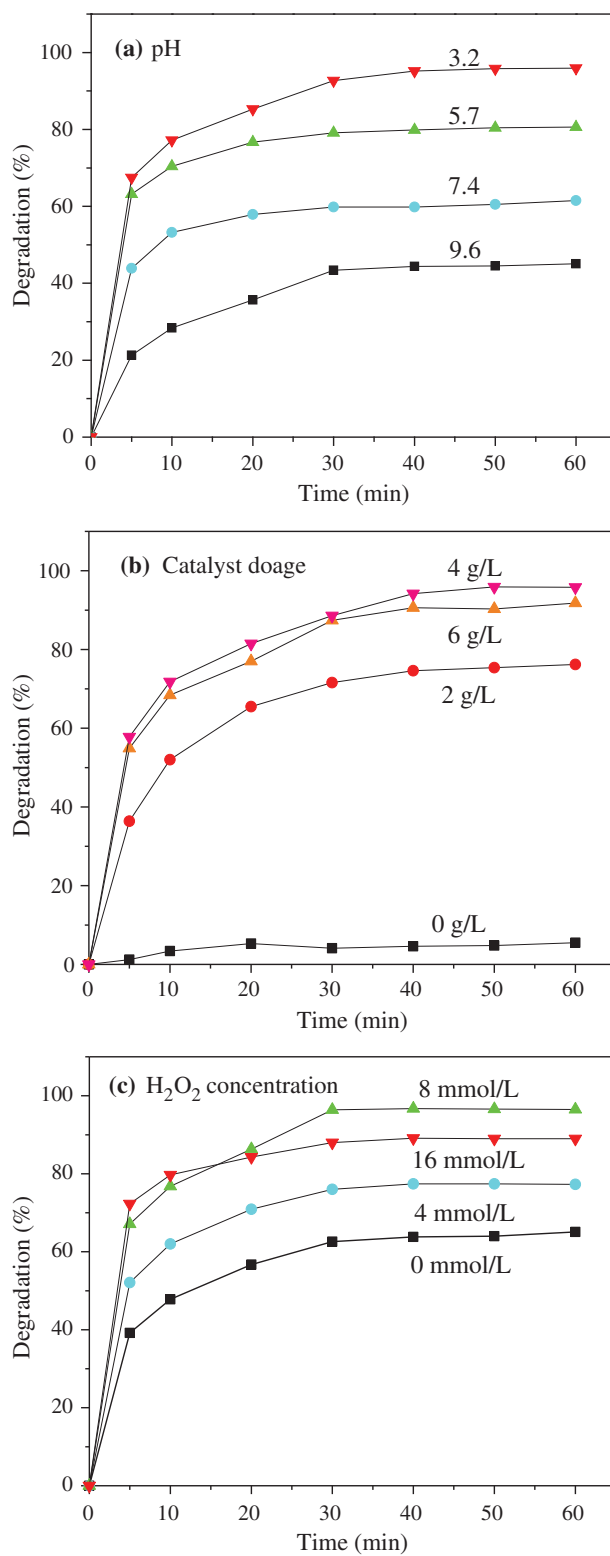
**Figure 4:** The hysteresis loop of the magnetic P zeolite

### 3.3 Degradation of Wastewater

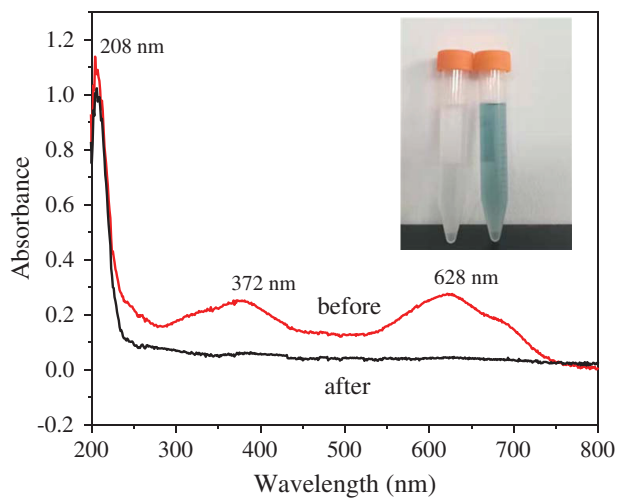
The magnetic P zeolite is used as a solid catalyst for the degradation of direct green B dye wastewater in Fenton-like reaction. The effects of the pH of solution, the dosage of catalyst, and the  $\text{H}_2\text{O}_2$  concentration on the degradation rate of direct green B dye wastewater are studied through single factor experiments to obtain the optimal parameters as shown in Fig. 5.

Fig. 5a shows that the influence of the solution pH from 3.2 to 9.6 on the degradation of direct green B dye when the catalyst dosage of magnetic P zeolite is 2 g/L and the concentration of  $\text{H}_2\text{O}_2$  is 4 mmol/L. It is found that the degradation rate rapidly reduces from 95.9% to 45.1% as the solution pH increases from 3.2 to 9.6 due to the decomposition of  $\text{H}_2\text{O}_2$  into  $\text{H}_2\text{O}$  and  $\text{O}_2$  under alkaline condition [24]. Much lower pH is easy to cause the corrosion of equipment, thus, the optimal initial pH is about 3.2. Fig. 5b displays that the effect of the catalyst dosage from zero to 6.0 g/L on the degradation of direct green B dye under the certain conditions, for instance, solution pH 3.2 and  $\text{H}_2\text{O}_2$  concentration of 4 mmol/L. The degradation rate of direct green B dye is ascend first from 5.5% (without catalyst) to 94.2% (4.0 g/L catalyst), and then descend from 94.2% to 91.6% (6.0 g/L catalyst) due to the fact that the catalyst is prone to aggregate into lump in the case of catalyst excess. Therefore, the optimum catalyst dosage is about 4.0 g/L. Fig. 5c shows the influence of  $\text{H}_2\text{O}_2$  concentration on degradation of direct green B dye under the constant pH 3.2 and catalyst dosage of 4.0 g/L. The degradation rate of direct green B dye increases from 65.1% to 96.3% with the increasing of  $\text{H}_2\text{O}_2$  concentration from 0 to 8 mmol/L, while the degradation rate declines to 85% as the concentration of  $\text{H}_2\text{O}_2$  rises to 16 mmol/L, suggesting that excessive  $\text{H}_2\text{O}_2$  traps hydroxyl radical ( $\cdot\text{OH}$ ) to generate peroxy radical ( $\text{HO}_2\cdot$ ) with lower redox potential than hydroxyl radical ( $\cdot\text{OH}$ ) so as to decrease the degradation rate of dye [25]. Hence, the optimal  $\text{H}_2\text{O}_2$  concentration is 8 mmol/L. It can draw an optimized reaction condition from Fig. 5. When the initial pH is about 3.2, the  $\text{H}_2\text{O}_2$  concentration is about 8 mmol/L, and the magnetic P zeolite catalyst dosage is about 4.0 g/L, there is the highest degradation rate of 96.3% for the direct green B dye over the magnetic P zeolite catalyst.

Fig. 6 shows the UV-vis spectra of direct green B dye before and after degradation over the magnetic P zeolite. The spectrum of direct green B dye presents three main characteristic absorption peaks at the wavelengths of 208 nm, 372 nm, and 628 nm. The strongest peak at 628 nm is assigned to be the absorption of azo chromophore, while the peaks at 208 nm and 372 nm are related to the absorptions of  $\text{E}_2$  and the naphthalene ring structure [26,27]. After degradation reaction, the peaks both 372 nm and 628 nm almost disappear, demonstrating that the azo chromophore and the naphthalene ring structure are



**Figure 5:** Effects of (a) pH, (b) Catalyst dosage, and (c) H<sub>2</sub>O<sub>2</sub> concentration on the degradation rate of direct green B dye



**Figure 6:** UV-vis spectra of direct green B dye before and after degradations treatment over magnetic P zeolite

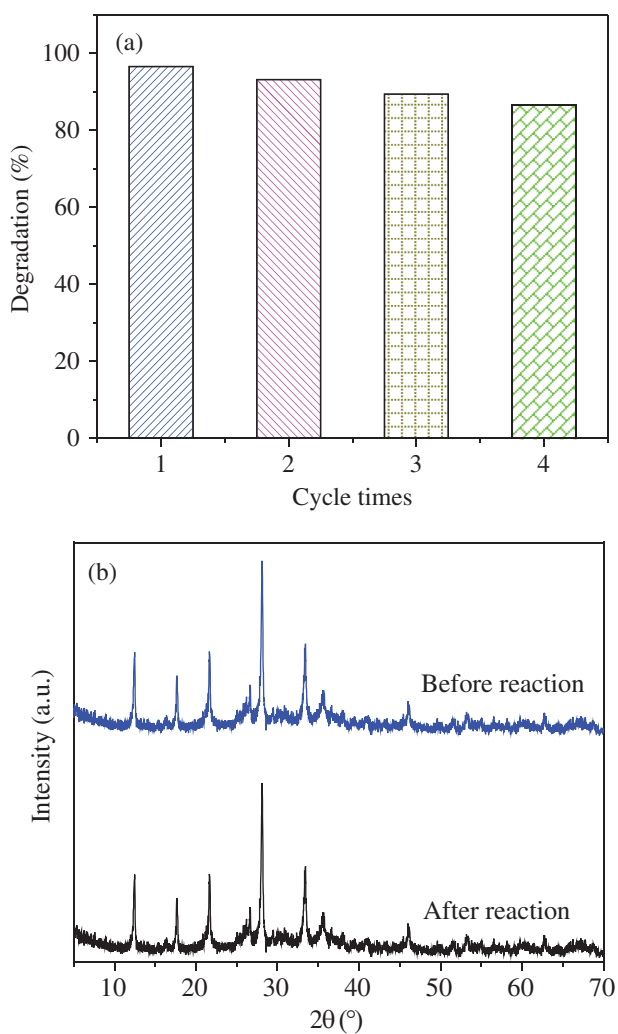


**Figure 7:** Stability of magnetic P zeolite of (a) cycle times, and (b) XRD patterns before and after degradation of direct green B dye

broken down to form the small molecule products, like phenol and aminobenzene which possess an absorption peak at 208 nm identified by high performance liquid chromatography-electrospray ionization-mass spectrometer (HPLC-ESI-MS) and gas chromatography-mass spectrometer (GC-MS) [28].

### 3.4 Stability of Magnetic P Zeolite

The stability of magnetic P zeolite is evaluated through four cycles under the optimal conditions as shown in Fig. 7. The degradation rate of direct green B dye decreases by 9.3% from initial 96.3 to 87% after four cycles, implying that the magnetic P zeolite still remains excellent catalytic activity in Fig. 7a. The XRD patterns of the magnetic P zeolite before and after degradations are almost same, indicating that the magnetic P zeolite has excellent stability as shown in Fig. 7b.

## 4 Conclusions

In this study, a magnetic P zeolite was directly synthesized by one-step hydrothermal method by use of industrial wastes of zinc slag and circulating fluidized bed fly ash. The magnetic P zeolite possessed superparamagnetism, a small coercive force of 70.02 G, a remanence of 0.05 emu/g, and a saturation magnetization of 3.85 emu/g. In addition, the magnetic P zeolite as a Fenton-like catalyst for dye wastewater treatment showed excellently catalytic degradation activity and high stability. The degradation rate of direct green B dye over the magnetic P zeolite catalyst approached to 96.3% under the conditions of initial pH of 3.2, H<sub>2</sub>O<sub>2</sub> concentration of 8 mmol/L, and catalyst dosage of 4.0 g/L. The as-synthesized magnetic P zeolite from both circulating fluidized bed fly ash and zinc slag realized the dual goal of “waste control by waste”, in which not only the industrial solid waste could be effectively reused, but also the magnetic P zeolite could be used as the catalyst for the treatment of dye wastewater in Fenton-like reaction.

**Acknowledgement:** This study was financially supported by the National Natural Science Foundation of China (No. 21676209), Key Research Development Project of Shaanxi Province (No. 2019GY-137) and the Cultivating Fund of Excellent Doctorate Thesis of Xi’an University of Architecture and Technology (No. 6040318008).

**Funding Statement:** The author(s) received no specific funding for this study.

**Conflicts of Interest:** The authors declare that they have no conflicts of interest to report regarding the present study.

## References

1. Li, Y., Yu, J. (2014). New stories of zeolite structures: their descriptions, determinations, predictions, and evaluations. *Chemical Reviews*, 114(14), 7268–7316. DOI 10.1021/cr500010r.
2. Li, Y., Li, L., Yu, J. H. (2017). Applications of zeolites in sustainable chemistry. *Chem*, 3(6), 928–949. DOI 10.1016/j.chempr.2017.10.009.
3. Yamaura, M., Fungaro, D. A. (2013). Synthesis and characterization of magnetic adsorbent prepared by magnetite nanoparticles and zeolite from coal fly ash. *Journal of Material Science*, 48(14), 5093–5101. DOI 10.1007/s10853-013-7297-6.
4. Fungaro, D. A., Yamaura, M., Craesmeyer, G. R. (2012). Removal from aqueous solution by zeolite from fly ash-iron oxide magnetic nanocomposite. *International Review of Chemical Engineering*, 4(3), 353–358.
5. Anunziata, O. A., Costa, M. G., Beltramone, A. R. (2006). Fe-ZSM-11 magnetic properties: its relation with the catalytic activity for NO<sub>x</sub> SCR with iso-butane and O<sub>2</sub>. *Applied Catalysis A: General*, 307(2), 263–269. DOI 10.1016/j.apcata.2006.03.053.

6. Cao, J. L., Fu, R., Liu, X., Tan, C. Y. (2007). Synthesis and characterization of P zeolite with Fe<sub>3</sub>O<sub>4</sub> core. *Chinese Journal of Inorganic Chemistry*, 23(12), 2065–2071.
7. Belviso, C., Agostinelli, E., Belviso, S., Cavalcante, F., Pascucci, S. et al. (2015). Synthesis of magnetic zeolite at low temperature using a waste material mixture: fly ash and red mud. *Microporous and Mesoporous Materials*, 202, 208–216. DOI 10.1016/j.micromeso.2014.09.059.
8. The China Report Hall. (2019). Statistical analysis of national zinc production from January to December 2018. <http://www.chinabgao.com/chanliang/284778.html>.
9. Hao, X. P., Han, J. W., Gao, Z. Q., Li, G. T. (2017). Comprehensive utilization of zinc smelting slag. *Inorganic Chemicals Industry*, 49(7), 57–60.
10. Qiu, R., Cheng, F., Huang, H. (2017). Removal of Cd<sup>2+</sup> from aqueous solution using hydrothermally modified circulating fluidized bed fly ash resulting from coal gangue power plant. *Journal of Cleaner Production*, 172, 1918–1927. DOI 10.1016/j.jclepro.2017.11.236.
11. He, P. Y., Zhang, Y. J., Chen, H., Han, Z. C., Liu, L. C. (2019). One-step synthesis of rod-shaped phillipsite using circulating fluidized bed fly ash and its application for removal heavy metal. *Ferroelectrics*, 547(1), 51–58. DOI 10.1080/00150193.2019.1592483.
12. Chen, X., Gao, J., Yan, Y., Liu, Y. (2017). Investigation of expansion properties of cement paste with circulating fluidized bed fly ash. *Construction and Building Materials*, 157, 1154–1162. DOI 10.1016/j.conbuildmat.2017.08.159.
13. Cao, J. L., Liu, X. W., Fu, R., Tan, Z. Y. (2008). Magnetic P zeolites: synthesis, characterization and the behavior in potassium extraction from seawater. *Separation and Purification Technology*, 63(1), 92–100. DOI 10.1016/j.seppur.2008.04.015.
14. Sathupunya, M., Gulari, E., Wongkasemjit, S. (2002). ANA and GIS zeolite synthesis directly from alumatrane and silatrane by sol-gel process and microwave technique. *Journal of the European Ceramic Society*, 22(13), 2305–2314. DOI 10.1016/S0955-2219(02)00042-0.
15. Bohra, S., Kundu, D., Naskar, M. K. (2013). Synthesis of cashew nut-like zeolite NaP powders using agro-waste material as silica source. *Materials Letters*, 106, 182–185. DOI 10.1016/j.matlet.2013.04.080.
16. He, P. Y., Zhang, Y. J., Chen, H., Han, Z. C., Liu, L. C. (2019). Low-energy synthesis of kaliophilite catalyst from circulating fluidized bed fly ash for biodiesel production. *Fuel*, 257, 116041. DOI 10.1016/j.fuel.2019.116041.
17. Zhang, M. J., Wang, M. L., Zhang, M. X., Maimaitiming, A., Pang, L. J. et al. (2018). Fe<sub>3</sub>O<sub>4</sub> nanowire arrays on flexible polypropylene substrates for UV and magnetic sensing. *ACS Applied Nano Materials*, 1(10), 5742–5752. DOI 10.1021/acsanm.8b01386.
18. Liu, Y., Yan, C. J., Zhang, Z. H., Wang, H. Q., Zhou, S. et al. (2016). A comparative study on fly ash, geopolymer and faujasite block for Pb removal from aqueous solution. *Fuel*, 185, 181–189. DOI 10.1016/j.fuel.2016.07.116.
19. Guo, C., Zou, J., Wei, C., Jiang, Y. (2013). Comparative study on extracting alumina from circulating fluidized-bed and pulverized-coal fly ashes through salt activation. *Energy & Fuels*, 27(12), 7868–7875. DOI 10.1021/ef401659e.
20. Liu, Y., Yan, C. J., Zhao, J. J., Zhang, Z. H., Wang, H. Q. et al. (2018). Synthesis of zeolite P1 from fly ash under solvent-free conditions for ammonium removal from water. *Journal of Cleaner Production*, 202, 11–22. DOI 10.1016/j.jclepro.2018.08.128.
21. Ali, I. O., El-Sheikh, S. M., Salama, T. M., Bakr, M. F., Fodial, M. H. (2015). Controllable synthesis of NaP zeolite and its application in calcium adsorption. *Science China Materials*, 58(8), 621–633. DOI 10.1007/s40843-015-0075-9.
22. Albert, B. R., Cheetham, A. K., Stuart, J. A., Adams, C. J. (1998). Investigations on P zeolites: synthesis, characterisation, and structure of highly crystalline low-silica NaP. *Microporous and Mesoporous Materials*, 21(1-3), 133–142. DOI 10.1016/S1387-1811(97)00059-0.
23. Jiang, J. L., Lu, X. Y., Huang, H., Duanmu, C. S., Zhou, S. M. et al. (2012). Preparation of magnetic Ni/wollastonite and zeolite P/Ni/wollastonite composite fibers. *Applied Surface Science*, 258(20), 8283–8288. DOI 10.1016/j.apsusc.2012.05.040.

24. Hsueh, C. L., Huang, Y. H., Wang, C. C. (2005). Degradation of azo dyes using low iron concentration of Fenton and Fenton-like system. *Chemosphere*, 58(10), 1409–1414. DOI 10.1016/j.chemosphere.2004.09.091.
25. Yang, C., Wang, D., Tang, Q. (2014). The synthesis of NdFeB magnetic activated carbon and its application in degradation of azo dye methyl orange by Fenton-like process. *Journal of the Taiwan Institute of Chemical Engineers*, 45(5), 2584–2589. DOI 10.1016/j.jtice.2014.06.010.
26. Shanmugam, S., Ulaganathan, P., Sivasubramanian, S., Esakkimuthu, S., Krishnaswamy, S. et al. (2017). Trichoderma asperellum laccase mediated crystal violet degradation-optimization of experimental conditions and characterization. *Journal of Environmental Chemical Engineering*, 5(1), 222–231. DOI 10.1016/j.jece.2016.11.044.
27. Mahmoodi, N. M., Arami, M., Limaee, N. Y., Tabrizi, N. S. (2005). Decolorization and aromatic ring degradation kinetics of Direct Red 80 by UV oxidation in the presence of hydrogen peroxide utilizing TiO<sub>2</sub> as a photocatalyst. *Chemical Engineering Journal*, 112(1-3), 191–196. DOI 10.1016/j.cej.2005.07.008.
28. Fan, H. J., Huang, S. T., Chung, W. H., Jan, J. L., Lin, W. Y. et al. (2009). Degradation pathways of crystal violet by Fenton and Fenton-like systems: condition optimization and intermediate separation and identification. *Journal of Hazardous Materials*, 171(1), 1032–1044. DOI 10.1016/j.jhazmat.2009.06.117.